Applied Nanoscience (2018) 8:2077–2092
https://doi.org/10.1007/s13204-018-0883-9

ORIGINAL ARTICLE

Photocatalytic and antibacterial potential of silver nanoparticles derived from pineapple waste: process optimization and modeling kinetics for dye removal

Shekhar Agnihotri[1,2] · Devendra Sillu[1] · Garima Sharma[1] · Raj Kumar Arya[3]

Received: 23 August 2018 / Accepted: 24 September 2018 / Published online: 27 September 2018

Abstract

Green chemistry offers several benefits over other synthesis routes of nanoparticles due to their eco-friendly attributes during their formulation as well as application stages. In the present study, an aqueous extract of *Ananas comosus* (Pineapple) peel waste was successfully exploited for the synthesis of ultra small (average size 14–20 nm) silver nanoparticles (AgNPs) without adding any reducing or stabilizing agents. Two major factors, i.e., concentration ratio between silver ion precursor versus peel extract and synthesis pH were found to be influential for achieving monodispersed and stable AgNPs. Biogenic AgNPs adorned with natural moieties demonstrated good photocatalytic activity against methylene blue (MB) dye under sunlight illumination for various conditions. The process variable, e.g., solution pH, initial MB concentration and contact time were optimized using response surface methodology (RSM) based on three levels Box-Behnken design. A maximum MB removal of 98.04% was achieved at optimized values of 9.96 pH, 40 ppm initial dye concentration and 173 min of contact time. The kinetics of MB removal was best fitted to its first order kinetic model ($R^2 = 0.996$) in concurrence with intraparticle diffusion-mediated adsorption. AgNPs were also found to be effective to kill pathogenic bacterial strains, *Pseudomonas aeruginosa* and *Bacillus subtilis* as characterized from zone of inhibition (ZoI) and viability tests. Undergoing photochemical reactions, the generation of reactive oxygen species (ROS) was elucidated as the major mechanism of AgNPs' toxicity modulating membrane permeability. This strategy is not only economically viable and environmentally benign, synthesized AgNPs were capable to remove methylene blue dye almost completely under ambient conditions through solar energy.

Keywords Green synthesis · Methylene blue · Response surface methodology · Photocatalytic activity · Reactive oxygen species · Antibacterial mechanism

Introduction

The rapid expansion of industries over last few decades has spurred a heavy release of organic pollutants into water streams. Out of several sources, industries related to chemical processing such as textiles, cosmetics, paints, plastics, pulp and paper generate a huge portion of dye effluents which eventually affect local water bodies (Khan and Malik 2018). Particularly, India is the largest exporter of dyestuffs after China where ~80% of the chemicals are involved in making dyestuffs and pigments and this amount is close to around 70,000 tons (Koyani et al. 2013; Shanker et al. 2017). It is estimated that 10–15% of the total dyes is lost in the effluent during industrial processes (Li et al. 2017); however, the actual amount of dyes discharged into the aqueous environment is expected to be much more. These dyes may deposit over the surface of water reducing the penetration

Electronic supplementary material The online version of this article (https://doi.org/10.1007/s13204-018-0883-9) contains supplementary material, which is available to authorized users.

✉ Shekhar Agnihotri
shekhar.agnihotri@thapar.edu

[1] Department of Biotechnology, Thapar Institute of Engineering and Technology, Bhadson Road, Patiala 147004, Punjab, India

[2] TIFAC Centre for Relevance and Excellence (CORE) in Agro and Industrial Biotechnology, Thapar Institute of Engineering and Technology, Bhadson Road, Patiala 147004, Punjab, India

[3] Department of Chemical Engineering, Thapar Institute of Engineering and Technology, Bhadson Road, Patiala 147004, Punjab, India

capacity of sunlight, and cause eutrophication to such an extent where the physicochemical and biological actions of aquatic life is severely affected (Akerdi et al. 2016; Vikrant et al. 2018). Though the toxicological consequences of dyes largely depend upon their complexed behavior and concentration, cationic dyes are known to be comparatively more lethal to aquatic ecosystem than their anionic counterpart (Hao et al. 2000). One of the most frequently used dyes in aforementioned industries is methylene blue (MB), which is well known for its hazardous effects to humans. A long term exposure to MB can cause burning to eyes eventually lead to its permanent damage. It may also cause breathing difficulties and some common symptoms like vomiting, nausea, profuse sweating, gastritis, diarrhea and mental confusion on inhalation (Ginimuge and Jyothi 2010). It is, therefore, very essential to eliminate MB from the water bodies via best possible ways.

Taking this into account, various approaches like adsorption, membrane filtration, ion exchange electrochemical and/or photochemical destruction, coagulation-flocculation have been explored for the effective degradation or removal of dyes (Forgacs et al. 2004; Hai et al. 2007). The use of biological methods (microbial degradation) are although environmental friendly, they are time consuming and may often seem ineffective due to the dye's toxicity, if present over 10% in wastewater reservoirs (Lokesh and Sivakiran 2014; Zhang and Wu 2014). Many of such approaches had initially shown some success while their utility over large scale, economic viability, and declining efficiency under practically relevant conditions urge for the development of some novel yet more effective techniques (Robinson et al. 2001).

With the emergence of nano-enabled hybrid technologies in recent times, researchers have gained new hopes of treating polluted wastewater over conventional methods (Mukherji et al. 2012; Lin et al. 2017). Metals like silver, gold, zinc oxide and titania at nanoscale exhibit a few extraordinary features i.e., high photocatalytic activity, quick oxidation, non-formation of polycyclic by-products, and bactericidal effects which make them an ideal candidate for the efficient treatment of polluted water (Agnihotri and Dhiman 2017; Agnihotri et al. 2018; Leng et al. 2018). Particularly, silver nanoparticles (AgNPs) are well acknowledged as 'plasmonic photocatalysts' where the excitation of localized polaritons at the nanoparticles' surface cause a paramount increase in the near-field amplitude at well-defined wavelengths (Awazu et al. 2008). The photocatalytic efficacy of AgNPs is largely governed by their size and shape which in turn, can be tuned by adopting different synthesis procedures (Agnihotri et al. 2014; Bharti et al. 2015). It is imperative that developing a facile method for synthesis of nano-silver would be of great importance, which actually dictates their long term efficacy in photocatalytic applications. For instance, the established chemical reduction based methods are robust, ease in operation and provide good control over size, shape and uniformity of AgNPs (Agnihotri et al. 2014). However, they lack in the two most important aspects, i.e., safety concern to the environment and potential toxicity of the released chemical by-products into waterways, which limit their sustainable application (Lee et al. 2007; Mukherjee et al. 2008).

A new epoch of green chemistry in nanobiotechnology has been emerged as a viable alternative, where natural products are gaining importance to be used as either reducing and/or stabilizing agents for silver than employing harsh chemicals (Akhtar et al. 2013; Saratale et al. 2018). A green synthesis of AgNPs emphasizes either on microbial using bacteria, algae, fungi, and yeasts or through plant extracts, which are considered as safe, environment friendly and biocompatible (Mukherjee et al. 2001). The special attention is given to the plant extracts which are easy to handle, isolate, store, which also serve as an ample reservoir of several biochemical products, employed as reductants (Sharma et al. 2009). Various plant species have been used till date to synthesize metallic nanoparticles including silver (Sharma et al. 2015). Among various plant sources, *Ananas comosus* (pineapple) is a sub-tropical fruit, which is known for its antioxidant properties. It is worth mentioning that nearly 50% of the entire fruit comprised of an outer skin and the central core part is termed as pineapple waste, which is the rich source of phenolic compound, ferulic acid, and vitamin A and C as antioxidant (Saraswaty et al. 2017). The mechanism for synthesis of nanoparticles is mainly devoted to various phytochemicals present in plant extracts which includes phenolics, carotenoids, alkaloids, flavonoids, and terpenoids (Akhtar et al. 2013). Particularly, the pineapple extract has been thoroughly studied for their characteristic phenolic and flavonoid compounds, which are known for its antioxidant and free radical scavenging properties (Hossain and Rahman 2011). The excessive amount of these phytochemicals present in the PW facilitates speedy reduction of ionic silver into AgNPs (Wei et al. 2011; Tokitomo et al. 2005).

In this study, a facile, economical and eco-friendly approach for synthesis of silver nanoparticles using *Ananas comosus* (pineapple) extract was investigated. We exploited the reduction potential of pineapple extract to synthesize small sized, stable nanoparticles under optimal ambient conditions. The as synthesized biogenic AgNPs were tested further for two major applications i.e., photocatalytic activity for the removal of methylene blue dye and antibacterial potential against *Pseudomonas aeruginosa* (gram-negative) and *Bacillus subtilis* (gram-positive) as opportunistic human pathogens. The photocatalytic activity of biogenic Ag NPs was evaluated under sunlight illumination varying three different parameters, pH of test solution, initial dye concentration, and reaction time. Response Surface Methodology (RSM) was adopted as a tool to find the important process

variables which would be directly affecting the dye decolorization potential of AgNPs under optimized conditions. The kinetics of dye removal via the photocatalytic effects of green AgNPs was modeled to various equations so as to achieve the best fit. Lastly, the strain-specific biocidal properties of AgNPs were also evaluated by determining their minimum inhibitory concentration (MIC), minimum bactericidal concentration (MBC) values and zone of inhibition tests. Conclusively, the utilization of pineapple waste for synthesizing AgNPs as a value-added product would not only be economically feasible, it would also be a sustainable solution to the environmental concerns associated with waste disposable.

Materials and methods

Silver nitrate ($AgNO_3$) and sodium hydroxide (NaOH) pellets were procured from Sigma-Aldrich, India while Methylene Blue (MB) dye was obtained from SD Fine Chemicals Pvt. Ltd, India. Antibacterial studies were carried out using *Pseudomonas aeruginosa* and *Bacillus subtilis* obtained from the microbial type culture collection (MTCC) at CSIR-IMTECH, Chandigarh, India. All analytical grade reagents were used without any additional purification. Deionized water was used throughout the studies for making aqueous suspensions with a measured resistivity 18.2 MΩcm.

Preparation of pineapple waste extract

Fresh pineapple waste (PW) collected from local juice vendor in Patiala district (30.3398°N, 76.3869°E) Punjab, India was cut into small pieces and kept in dark for overnight. Next day, the PW was washed under tap water followed by deionized water twice and then dried in hot air oven at 55 °C for 24 h. A grinded form of dried pineapple waste was obtained using a kitchen mixer, subsequently sterilized under UV chamber for 30 min and kept in sealed plastic bags. Nearly 30 g of pineapple waste was suspended in 300 mL of DI water and kept in water bath at 60 °C for an optimal duration of 40 min. The resulting mixture was allowed to cool down, filtered through Whatman filter No. 1 and centrifuged at 5000 rpm for another 10 min. The pellets were then discarded and resulting supernatant was again passed through 0.22 µ syringe filter to remove any impurities, if remain. The final solution was considered as the pineapple waste extract, which was stored at 4 °C until further use.

Biogenic synthesis of silver nanoparticles and characterization

In a typical synthesis protocol, the desired concentration of $AgNO_3$ solution (5 mL) was slowly introduced into 45 mL of the pineapple extract with constant stirring at room temperature under dark conditions. To study the effect of pH, synthesis of AgNPs was conducted adjusting pH of pineapple waste extract to 4, 6, 8 and 10, as reported in our previous work (Agnihotri et al. 2014). The reduction capacity of pineapple waste extract to synthesize silver nanoparticles was evaluated where five different concentrations of $AgNO_3$ were introduced in the PW extract with 1:9 ratio (v/v) such that the final Ag conc. in resulting mixture was obtained as 0.5, 1.0, 1.5, 5, and 9 mM. The characterization of as synthesized samples was primarily done using UV–Vis spectroscopy (Shimadzu UV-2600, Japan) and dynamic light scattering analyses for selecting the best composition of reactants responsible for synthesized small, stable silver nanoparticles.

The optimized (5 mM Ag, final conc.) AgNP sample was further characterized in detail as follows. FTIR (Bruker Inc., Germany) spectroscopy was done to compare the functional moieties present on pineapple extract and over AgNPs' surface after synthesis. The crystallinity of AgNPs was analyzed using X-Ray diffraction diffractometer (Philips Xpert PRO, The Netherlands). For XRD analysis, sample was prepared by coating colloidal AgNPs on to silanized glass surface following our established method (Agnihotri et al. 2013). Since the analysis was done at slow scan speed (0.017° per 25.18 s.) for detecting the presence of any impurities over AgNPs, the background signals of glass substrate were inevitable. The morphology and size of AgNPs was determined using high-resolution transmission electron microscopy (HRTEM, JEOL 2100, Japan). For HRTEM sample preparation, nearly 8 µL of AgNP suspension was sonicated for 30 s and immediately dropped over carbon coated Cu grids. The grids were dried using IR lamp for 15–20 min, just prior loading into TEM chamber.

Photocatalytic decolorization of methylene blue dye

The photocatalytic potential of synthesized AgNPs was evaluated using methylene blue as a model dye. Several test solutions of MB dye viz. 10, 20, 30, 40 and 50 ppm were prepared from its stock solution. Briefly, 0.2 mL of synthesized AgNP suspension was introduced into 2.8 mL of dilute MB solutions prepared at different concentration separately, and the resulting mixture were exposed to direct sunlight for different time periods under continuous stirring. The radiation flux density (Wm^{-2}) of natural sunlight was measured using Pyranometer (CMP-11, Kipp and Zonen, The Netherlands) over a month period (April, 2018) having wavelength range of 285–1100 nm. Direct sunlight with a mean value of irradiance of 787 ± 25 Wm^{-2} was reported in mid-day hours (11AM–2PM) during which entire photochemical experiments were conducted. The concentration of MB in the supernatant was determined using UV–visible spectrophotometer after filtering the MB-AgNPs mixtures through 0.22 µm syringe filter so as to remove the photocatalyst particles. The photocatalytic

potential of biogenic AgNPs after desired time intervals (5–180 min) was analyzed using the following details;

$$\text{Decolorization}\ (\%) = \frac{C_0 - C}{C} \times 100,$$

where C_0 and C (both in mg L^{-1}) are the initial ($t = 0$) and remaining concentration (after any irradiation time t) of MB in solution, respectively.

The impact of four major process variables affecting dye decolorization, i.e., the effect of (A) pH (B) dye conc. (C) AgNPs conc. and (D) contact time was determined individually as per following details (Supporting Info, Section-S1). The optimization of dye decolorization was further done using Response Surface Methodology (RSM) employing Design Expert software version 6.0.6 (STAT-EASE, USA) (Supporting Info, Section-S2). The kinetics of photocatalytic decolorization of MB dye was determined for its practical relevance and applications. In this study, four different kinetic models, i.e., first order, pseudo-first order, second order, and pseudo-second order were tested to analyze the photocatalytic decolorization of MB by AgNPs.

Antimicrobial activity

The antimicrobial activity of biogenic Ag NPs was evaluated against two pathogenic microbial strains of *Pseudomonas aeruginosa* (gram-negative) and *Bacillus subtilis* (gram-positive). All standard antimicrobial assays, e.g., minimum inhibitory concentration (MIC), and minimum bactericidal concentration (MBC) and zone of inhibition (ZoI) tests were conducted as reported earlier (Agnihotri et al. 2014). The presence of light conditions on photochemical performance of AgNPs was evaluated to elucidate the mechanism of antibacterial action. For this, independent batch cultures of *P. aeruginosa* and *B. subtilis* (each 100 mL volume, 10^5 CFU mL^{-1}) were introduced with 5.0 µg mL^{-1} AgNPs suspension and exposed to sunlight irradiation for 3 h, followed by incubating at 37 °C for next 6 h under shaking conditions. Another set of experiments were conducted by treating both the strains with AgNPs but were kept under dark conditions for similar duration (3 h in dark, followed by 6 h of incubation). After required washing steps, the amount of proteins' leakage from the treated bacterial cells was quantified as reported elsewhere. All experimentations were done in triplicates and the mean outcome is presented.

Results and discussion

Characterization and optimization of AgNP synthesis

It is well recognized that plants mediate synthesis of AgNPs via their inherent metabolites like terpenoids, alkaloids, phenolic acids, polyphenols and proteins, which act as reducing as well as stabilizing agents (Raveendran et al. 2003). All plants differ in the concentration and composition of these metabolites, which can control the size and morphology of AgNPs (Mittal et al. 2013). Thus, an optimal concentration ratio between silver precursor: plant extract would be of prime importance to elucidate the reducing potential of PW extract for synthesizing ultra small and stable silver nanoparticles (Agnihotri et al. 2018). For this, five different Ag concentrations were introduced in PW extract with 1: 9 ratios (v/v) such that the final Ag conc. in resulting AgNPs solution was obtained as 0.5, 1.0, 1.5, 5, and 9 mM. The formation of Ag NPs was observed visually as the color of PW extract changed instantly from light yellow to deep yellow upon adding first few drops of silver ion precursor. The color of all working solutions was further changed to deep brown to wine red, depending upon Ag concentration (Fig. 1a). Synthesis of AgNPs was validated qualitatively through UV–Vis spectroscopy showing an extinction peak in the range of 390–410 nm, owing to their Surface Plasmon resonance (SPR) effect (Agnihotri et al. 2015, 2013, 2014).

The intensity of the color was increased progressively over the time duration of 1–30 min. For all Ag concentrations, no further change in peak intensity was observed even up to 24 h of reaction time, which is an indicative of the successful completion of nucleation and growth phases of colloidal silver (Agnihotri et al. 2014). As shown in Fig. 1b, owing to their high surface energies, the primary silver nuclei formed after plant mediated reduction acted as templates for subsequent crystal growth of silver atoms (Thanh et al. 2014). These primary nuclei underwent coalescence forming bigger silver clusters and ultimately lead to the synthesis of stable silver nanoparticles upon Ostwald ripening (Agnihotri et al. 2012). An increase in total silver (as ions) concentration of the mixture led to a red shift in the extinction peak of UV–Vis spectra (Fig. 1c). For instance, the characteristic SPR peak with the colloidal solution having 0.5 mM, 1 mM, 1.5 mM, 5 mM, and 9 mM as final silver conc. was observed at 400.5, 411, 414, 416, and 436 respectively (at neutral pH). All suspensions showed a narrow size distribution except that with either lowest (0.5 mM) or highest silver content (9 mM) and hence, were not proceed further. Similar trend was obtained through dynamic light scattering (DLS) results where AgNPs suspensions with 1, 1.5 and 5 mM silver content showed a comparative lower hydrodynamic size of NPs as 17.5, 14.5 and 18. 8 nm, as compared to 31.8 and 41.2 nm in case with 0.5 and 9 mM suspensions (Fig. 1d). As the concentration of $AgNO_3$ was increased beyond 1 mM, the extinction peak started becoming broader which can be ascribed to increase in the size of nanoparticle. DLS data were found in good accordance with

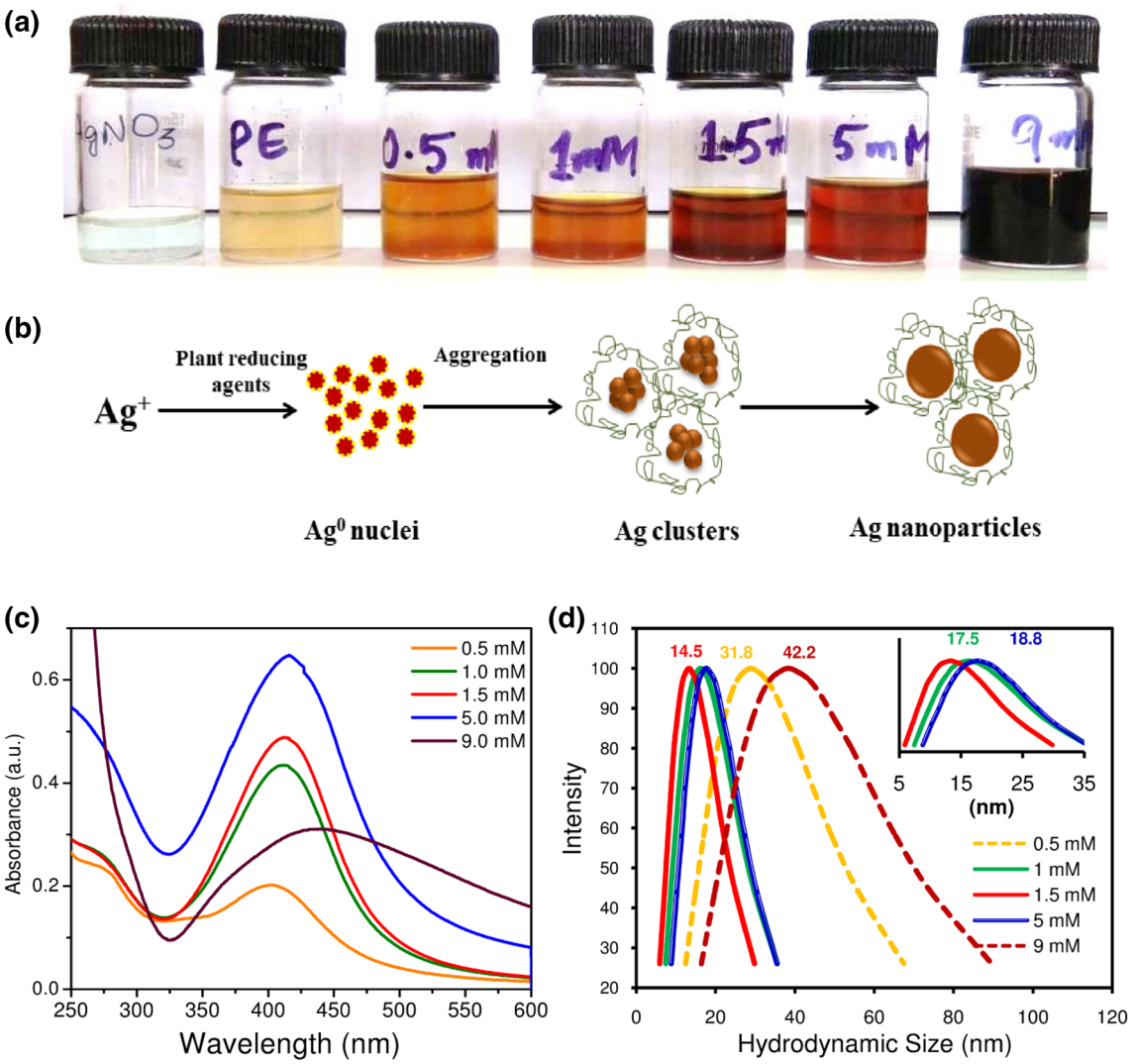

Fig. 1 **a** Photographic representation (left to right) of $AgNO_3$ solution, pineapple waste extract, synthesized AgNPs having final Ag conc. as 0.5, 1, 1.5, 5, and 9 mM. **b** A hypothesized mechanism of AgNPs synthesis through pineapple waste extract. **c** UV–Vis spectra and **d** Dynamic light scattering (DLS) analyses of as synthesized silver nanoparticles (the coincided curves are magnified in the inset image)

the abnormal extinction spectrum (red shift, broad peak) for 9 mM AgNP colloids, which can be ascribed to significant agglomeration of silver at higher concentrations. Based on these observations, the synthesis protocol with 1.0 mM final Ag conc. at an optimum duration of 30 min was adopted for further optimization.

Apart from Ag: PW extract concentration ratios, the impact of pH during AgNPs synthesis was also investigated at 4, 6, 8, and 10 pH of PW extract while keeping a constant Ag concentration of 1 mM (Fig. 2). All working solutions, regardless of their pH participated in synthesis of nanoparticles where peak absorbance of the active ingredients of extract was decreased (range 200–250 nm) while new peaks corresponding to silver nuclei increased (range 360–400 nm) as revealed through time-resolved UV–Vis spectroscopy. The peaks of silver nano clusters got sharper over a period from 5 to 30 min. As predicted, the PW extract adjusted with pH 4 could not stabilize silver nuclei and despite an initial indication of the formation of AgNPs, it could not be translated later in form of a distinct silver peak (Fig. 2a). Similar effect was observed with the extract of Pineapple waste maintained at 6 pH, where large aggregates of silver with broad size distribution was anticipated than in their nanoparticulate form (Fig. 2b). This was further evidenced by leaving all suspensions undisturbed for 24 h, where silver was entirely precipitated in case with pH 4 sample, a little precipitation with pH 6, while no precipitation was observed with that of either 8 or 10 pH. Interestingly, at pH 8 and 10,

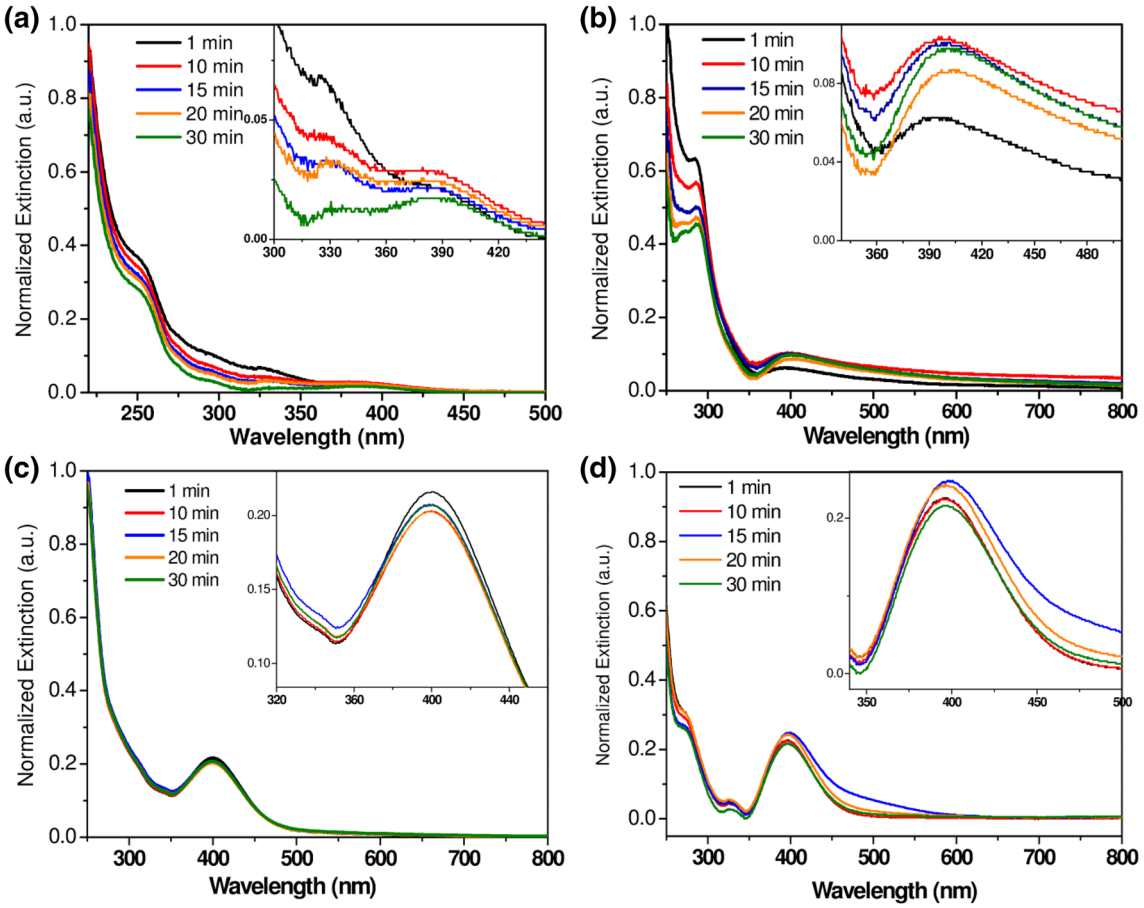

Fig. 2 Impact of the pH of PW extract on synthesis of silver nanoparticles. A time-resolved UV–Vis spectroscopy of all working solutions of PWE adjusted to a pH **a** 4, **b** 6, **c** 8 and **d** 10 was done over a duration of 30 min (Inset images are shown as magnified view of the coincided curves)

the absorbance of peak within 395–400 nm did not gradually red shifted while the peaks slowly reduced its intensity over duration of 30 min. This is in good agreement with earlier reports (Kasuya et al. 2004; Thanh et al. 2014) which clearly indicates that the colloidal system was not undergoing Ostwald ripening anymore, which might result in further increase in size of Ag nanoparticles. Instead, after an initial nucleation phase, the presence of active metabolites at alkaline pH started contributing as capping agents, preferentially to stabilize them. For colloidal Ag synthesized at pH 8 and 10, both of them resulted in sharp peaks with a calculated full width at half maximum (FWHM) values of 78 and 65, respectively. A symmetric, sharp absorptive peak with lower FWHM values indicates the existence of the narrow size distribution (monodispersed system) of AgNPs (Peng et al. 2010; He et al. 2001). Hence, further studies were conducted maintaining the pH of colloidal AgNPs as 10 an optimal pH.

The FEG-TEM micrograph of silver nanoparticles synthesized using pineapple waste extract under aforementioned optimized conditions is shown in Fig. 3a. The results corroborated well with UV–Vis spectroscopy and DLS data where ultrasmall, spherical AgNPs in the size range from ~ 11 to 26 nm (average size 16.08 ± 0.10 nm) were found with good monodispersity (Fig. 3b). The absence of undesired nanostructures, i.e., large clusters or irregularly shaped particles is ascribed to the controlled conditions during AgNPs synthesis, which confirms our protocol to be a facile, easy, and reproducible method without involving any toxic chemicals. The zeta potential measurements showed a value of − 26 mV suggesting higher stability of AgNPs with an overall negative charge on their surface (Agnihotri et al. 2013). The average dispersity of nanoparticles (i.e., polydispersity index) invariably remain unchanged in alkaline conditions such that they can be stored nearly about 6 months without significantly affecting their stability. The crystalline behavior of green synthesized silver nanoparticles was determined using X-Ray diffraction (XRD) analyses (Fig. 3c). The characteristics Bragg reflections with 2θ values at 38.18°, 44.25°, and 64.72° can be indexed to (111), (200), and (220) lattice planes of a typical fcc crystals of

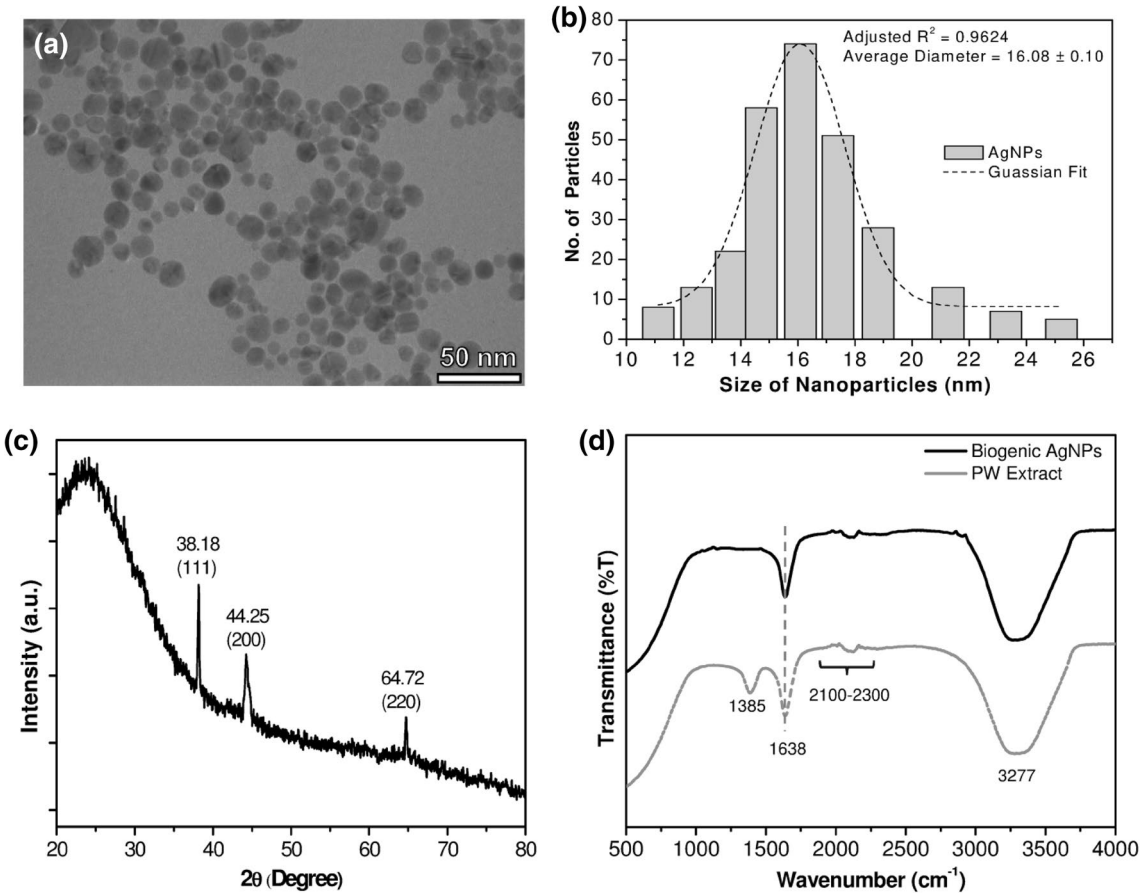

Fig. 3 **a** FEG-TEM micrograph of AgNPs synthesized under optimal parameters (final Ag conc. 1 mM, pH 10), **b** size distribution of synthesized AgNPs with Gaussian fit, **c** XRD data showing its peaks and crystalline planes. **d** FTIR spectra of PW extract and biogenic AgNPs

silver, respectively (Agnihotri et al. 2013). The absence of other peaks also evidenced high purity of AgNPs synthesized using biological route.

The FTIR spectra of PW extract and synthesized AgNPs are presented in Fig. 3d. Comparing both the spectra, similar peaks were observed at most regions reflecting the fact that functional mioeties present on the PW extract have become an integral part of nanoparticles (Nadagouda et al. 2014). This can only happen when the biomacromolecules present in PW extract would act as capping agents for efficient stabilization of colloidal Ag during synthesis. For instance, the strongest peak appeared at 3277 cm^{-1} is an indicative of O–H stretching, while a peak at 1638 cm^{-1} can be ascribed to the C=O stretching vibrations (Agnihotri et al. 2012). This clearly indicates the existence of hydroxyl and carbonyl groups on AgNPs' surface. Furthermore, the absorptive bands within 2100–2300 cm^{-1} were also observed in IR spectra, which comprise of N=O stretching, CH_3 stretching, O–N=O bending, and C=C stretching (Kora et al. 2012). One of the plausible explanations for the existence of these peaks would be the presence of amino acids, organic acids and carbohydrates in the PW extract. Interestingly, the band observed at 1385 cm^{-1} in the PW extract, assigned to C–N stretching was completely absent in case with AgNPs. This provided us a strong evidence to understand the stabilization behaviour of AgNPs where Ag atoms would have strongly coordinated with C–N bond such that it quenched their vibrational frequencies, and hence the characteristic peak was vanquished.

Photocatalytic degradation of dye: operational parameters

Out of several factors, which may affect the decolorization of MB dye, four major operational parameters, i.e., effect of pH, effect of initial dye concentration (ppm), effect of AgNP conc. (mM), and effect of irradiation time (min) were selected to conduct photocatalytic studies. As shown in Fig. 4a, the photocatalytic decolorization of MB (initial conc. 40 ppm) was evaluated over a wide pH range from 3 to 11 for about 3 h of contact time under natural sunlight conditions. The pH was likely to influence the decolorization potential of silver nanoparticles considering the fact that the ionization potential of MB strongly depends upon the solution pH whereas,

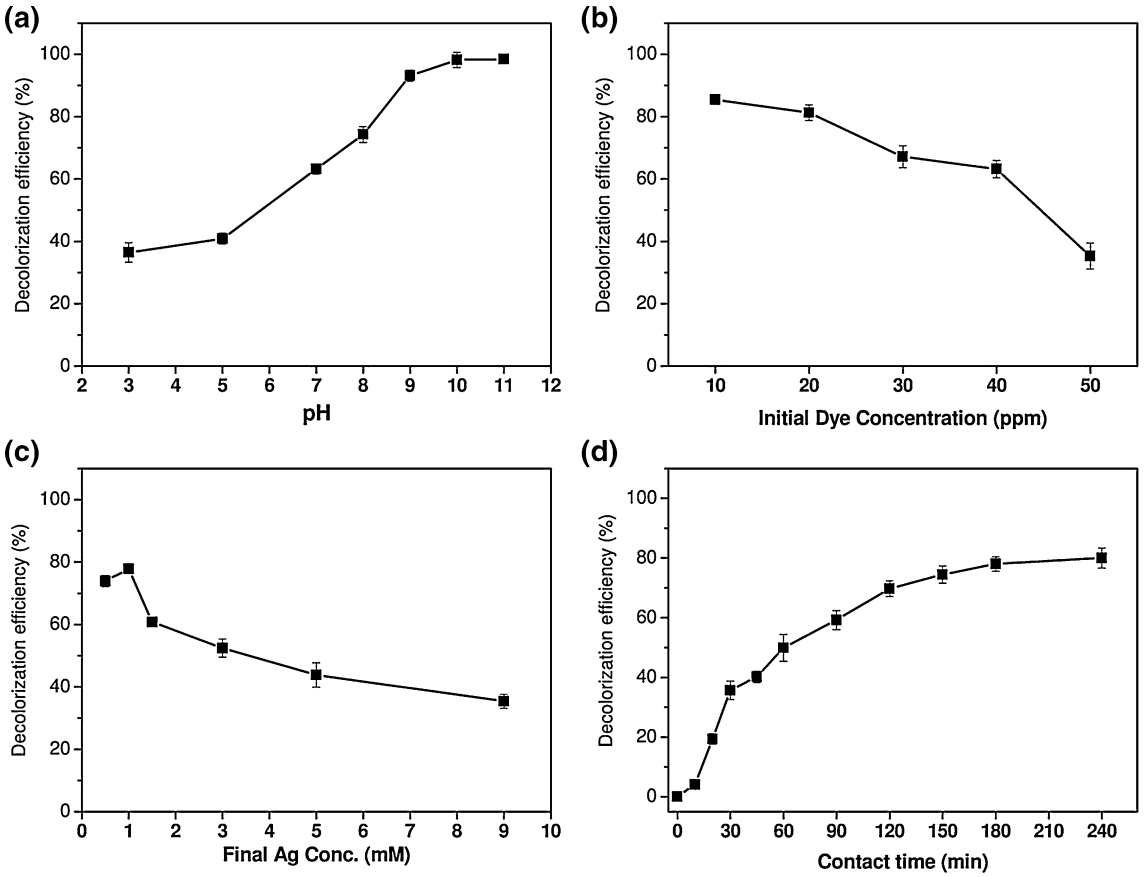

Fig. 4 The effect of operational variables **a** working pH, **b** initial dye concentration (ppm), **c** AgNP concentration (mM) and **d** Irradiation time on decolorization efficiency of AgNPs. The experiments were conducted in triplicates and mean values are reported with standard error

the colloidal stability of AgNPs is also a pH dependent phenomenon (Sahoo and Gupta 2012). It is evident that decreasing pH of the MB working solution resulted in the reduction of decolorization efficiency of AgNPs from 63.2% at neutral pH to 40.8% and 36.4% at pH 5 and 3, respectively. In contrast to this, increasing alkalinity of the MB solution gave rise to enhanced decolorization efficiency to 74.2%, 93.1%, and 98.1% at their respective pH of 8, 9, and 10. Further increase in pH to 11 did not significantly increase the decolorization efficiency and thus, a pH of ~ 10 was considered to be an optimal pH. The above trend can be explained by a proposed mechanism of oxidative dissolution of AgNPs under a wide range of pH conditions.

$$4Ag^0 + O_2 \xrightarrow{\text{Dissolution}} 2Ag_2O \quad (1)$$

$$2Ag_2O + 2H^+ \xrightarrow{\text{Acidic pH}} 2Ag^+ + H_2O \quad (2)$$

$$Ag_2O + 2OH^- + H_2O \xrightleftharpoons{\text{Alkaline pH}} 2[Ag(OH)_2]^- \quad (3)$$

As mentioned above, the interaction of AgNPs with aqueous suspension of MB is initiated through their oxidative dissolution under ambient conditions. The silver atoms (Ag^0) at nanoparticles' surface inevitably react with dissolved oxygen resulting in the formation of silver (I) oxide, Ag_2O layer at sub-nanoscale (Tayade et al. 2009). This silver oxide layer act as a reservoir of silver ions, which get released into the system till the oxidative dissolution of Ag_2O continues, at neutral pH. However, under acidic conditions, the protonation of Ag_2O layer accelerates the oxidative dissolution of silver nanomaterials, which can be manifested through a high conc. of Ag^+ ion released into the system. A high dissolution of AgNPs would be the responsible factor for alleviating their colloidal stability and in turn, their photocatalytic efficacy as well. This explanation corroborates well with an earlier report where a much higher release of Ag^+ from colloidal AgNPs into solution has been investigated at acidic pH, which affected their colloidal stability (Peretyazhko et al. 2014). On the other side, Ag_2O layer in the excess of hydroxyl ions (i.e., alkaline conditions) result in the formation of $[Ag(OH)_2]^-$, a highly unstable compound which reversibly gets converted into Ag_2O. This indicates

that the existence of Ag_2O layers over AgNP surface stabilize more under alkaline conditions, which restrict their oxidative dissolution by lowering the release of Ag^+ and eventually maintained the colloidal stability of AgNPs.

A higher color removal at alkaline pH can also be explained on the basis of greater interactions between cationic dye (MB) molecules and negatively charged AgNPs. The activation of AgNPs under sunlight illumination ($h\upsilon$) produces electron–hole pairs ($Ag^0 + h\upsilon \rightarrow h^+_{VB} + e^-$) which may either act as strong oxidizing ($h^+_{VB} + OH^- \rightarrow OH\cdot$) or reducing agents ($O_2 + e^- \rightarrow O_2^-$). Particularly, under an excess of hydroxyl (OH^-) environment, the hole pair formation on the catalyst surface generates high amount of hydroxyl free radicals ($OH\cdot$) upon photo-oxidation. The hydroxyl free radicals eventually participate as main oxidizing species for degradation of MB. Hence, further studies were performed at an alkaline pH of 10 so as to achieve maximum decolorization.

The effect of initial dye concentration (MB, in ppm) was investigated as another important parameter for evaluating the photocatalytic efficacy of silver nanoparticles. As shown in Fig. 4b, the decolorization efficiency gradually decreased with increasing an initial MB concentration up to 40 ppm. Further increase in initial dye concentration (50 ppm) showed a drastic change where decolorization efficiency of AgNPs was decreased up to 35.4%. It is a known fact that MB decolorization is a light sensitive phenomenon. With increasing dye concentration, a multilayer adsorption of dye molecules over catalytic surface decreases the penetration capacity of UV-light to induce photo-oxidation. As a result, the number of hydroxyl free radicals attacking MB molecules would reduced abruptly resulting in the lowering of decolorization efficiency. It implies that the number of hydroxyl free radicals should increase in proportion with MB concentration for achieving similar efficacy. However, the experiments were performed at a constant dose of AgNP (1 mM) where the number of $OH\cdot$ free radicals generated would remain same irrespective of increasing MB concentration (Tayade et al. 2009). This might also contributed towards lowering in the color removal capability of AgNPs.

In a similar way, the effect of catalytic dose (initial Ag conc.) on MB decolorization was evaluated at an optimized pH of 10 with a contact time of 180 min (Fig. 4c). It was observed while increasing the catalytic dose of AgNPs also enhanced the decolorization efficiency from 73% (0.5 mM, as final Ag) to 78% (1 mM, as final Ag), further increase in catalytic dose caused a greater reduction in photocatalytic activity even up to the extent of 43.5% and 35.4%, in case with 5 and 10 mM AgNPs, respectivly. This happened because light could not penetrate deeply into a suspension with high concentration of nanoparticles where multiple backscattering of light at fluid's interface apparently decreased the overall absorption of light (Hogan et al. 2014). At last, the impact of irradiation time on decolorization efficiency was studied upto a duration of 240 min (Fig. 4d). The result data showed an increase in decolorization (~79%) up to 180 min, afterwards no significant change was observed till 240 min.

Statistical optimization using response surface methodology (RSM)

RSM was employed to study the impact of three independent variables, i.e., working pH, initial dye concentration (ppm), and contact time (min) on decolorization of MB. A one-to-one interaction among each process variables are graphically represented by three-dimensional response surface plots and two-dimensional contour plots, while the responses were predicted and the optimum values for decolorization were determined as shown in Table 1. The absolute equation in terms of the actual factors with significant terms, which affected the decolorization potential of AgNPs are represented as follows:

$$\begin{aligned}\text{Decolorization (\%)} = {} & 29.66173 + 4.80716A - 2.82514B \\ & + 0.35554C - 0.13190A^2 + 0.017261B^2 \\ & - 1.62634E - 003C^2 + 0.15548AB \\ & + 0.022409AC + 1.03588E - 003BC\end{aligned}$$

The competence of the experimental data was interpreted by the analysis of variance (ANOVA) as shown in Table S-2, Supporting info. The ANOVA of second order

Table 1 RSM based Box-Behnken experimental design for the independent variables and their corresponding response [Dye decolorization (%)] for MB decolorization by AgNPs

Run	pH	Dye Conc. (ppm)	Time (min)	Dye decolorization (%)	
				Actual	Predicted
1	7.00	10.00	180.00	85.42	82.61
2	10.00	40.00	95.00	88.33	85.67
3	10.00	25.00	180.00	96.51	99.87
4	7.00	25.00	95.00	59.44	60.68
5	7.00	25.00	95.00	58.48	60.68
6	4.00	25.00	10.00	10.39	7.04
7	4.00	40.00	95.00	17.27	17.82
8	7.00	25.00	95.00	60.60	60.68
9	7.00	10.00	10.00	45.57	46.27
10	7.00	40.00	180.00	62.69	61.99
11	4.00	10.00	95.00	52.40	55.07
12	10.00	25.00	10.00	49.61	49.46
13	4.00	25.00	180.00	34.43	34.59
14	7.00	40.00	10.00	17.55	20.37
15	10.00	10.00	95.00	95.48	94.94
16	7.00	25.00	95.00	62.71	60.68
17	7.00	25.00	95.00	62.13	60.68

quadratic polynomial model for dye decolorization indicated a high significance of the generated model since F value of 126.65 was obtained with a p value less than 0.0001 at 95% confidence level. The lack of fit (variation of data around the fitted model) F value of 5.73 corroborates well with the obtained R^2 value (0.9939) indicating a great correlation between predicted and experimental values of operational parameters. It was depicted that the change in response was certainly due to a real cause, i.e., change in the independent variables, not by any kind of error or noise. The values of Adj-R^2(0.9860) and Pred-R^2 (0.9190) were also in reasonable agreement where the variance was found to be less than 0.2. Acceptable precision measures the ratio of signal to noise, where a ratio better than 4 is considered good for accepting a model. In the current study, it was obtained to be 39.155, thus indicating that this model is useful to navigate the design space.

The ANOVA for the coefficients of regression model for dye decolorization is shown in Table S3 (Supporting info). Among three variables, the pH of solution (A) marked the greatest influence on dye decolorization (%) followed by irradiation time (C) and initial MB concentration (B) as manifested by their F values of 607.02, 317.98 and 113.23, respectively. Interestingly, none of the other quadratic terms (A^2, B^2) or interactions between the independent variables (AB, BC, AC) demonstrated any significant effect on MB removal, except C^2. Initial dye concentration has low negative effect whereas working pH and irradiation time has comparatively high positive effect on dye decolorization. Furthermore, the model suitability was confirmed by investigating the residuals, i.e., difference between the predicted and observed response as shown in Section-S3 (Supporting info).

To perceive the effect of individual independent variables and their interaction on dye decolorization, 3D response surfaces plots and 2D contour plots were plotted by keeping one variable constant within the experimental ranges (Fig. 5). As shown in Fig. 5a, the interaction effect of pH and initial MB concentration on dye decolorization rate was plotted at a constant irradiation time of 95 min. It is evident that the decolorization efficiency (%) increased with increasing pH regardless of the initial concentration of MB dye where the maximum effect was found in the pH range 8–10. At alkaline pH, the negatively charged AgNPs becomes more stabilized and hence, there are more likely to interact with oppositely charged MB molecules. Earlier, it was depicted through Fig. 4 that the decolorization efficiency decreased gradually while increasing initial dye concentration up to 40 ppm and abruptly thereafter. This trend was further validated and tuned through statistical optimization (Fig. 5 a, c). A good decolorization efficiency of AgNPs can be achieved considering an initial MB conc. within 20–35 ppm under varying solution pH and irradiation time conditions.

Figure 5b demonstrates the interaction plot of pH and irradiation time at an initial dye concentration of 25 ppm. The MB dye decolorization was significantly altered by change in both irradiation time and pH. The dye decolorization showed an increased efficiency with increasing irradiation time. As a fact, the photocatalytic reaction triggers soon after an initial adsorption of MB molecules over catalyst's surface, resulting in the formation of hydroxyl free radicals. Since the catalytic dose is constant, more number of free radicals would be available at lower initial MB concentrations. Hence, the decolorization efficiency decreased at higher initial MB concentrations. The dye decolorization also considerably increased with increasing pH where the role of hydrogen bonding for enhancing interaction between dye molecules and photocatalyst surface is anticipated. Figure 5c shows the interaction effects of irradiation time and initial MB concentration on dye decolorization. It is evident that the decolorization efficiency decreased slowly at lower irradiation time with increasing initial MB concentration. In fact, larger exposure would lead to the production of more number of hydroxyl free radicals which are accountable for oxidizing MB molecules and hence more decolorization. The optimal change in decolorization was significant in the range from 10 to 60 min as irradiation time below 25 ppm as the initial MB concentration. The maximum decolorization rate of > 81% was observed at 10 ppm MB concentration and irradiation time between 130 and 180 min. All the observations were in accordance with the preliminary experiment results.

Process optimization and kinetic studies of dye decolorization

The optimization was targeted considering three important prerequisites, i.e., treating the highest initial MB concentration while minimizing irradiation time (faster) under a practically relevant pH. For the given experimental conditions, the maximum decolorization (99.9%) of MB was predicted for a photocatalytic system where an initial MB concentration of 40 ppm was treated with AgNP suspension containing 1 mM as final Ag conc. adjusted to ~ 10 pH and was irradiated to a total duration of ~ 173 min. It was clearly observed that the characteristic absorbance peak of MB dye (~ 664 nm) decreased continually with respect to irradiation time indicating its removal as a consequence of either adsorption over AgNPs' surface or via catalytic degradation (Fig. 6a). As stated earlier, the photocatalytic degradation involves strong interactions between free hydroxyl (OH·) radicals and the chromogenic functional moieties of methylene blue, resulting in its N-demethylation. As shown in Fig. 6b, the kinetics of photocatalytic dye removal was calculated by plotting the ratios of instantaneous: initial concentration of MB (C/C_0) as a function of contact time up

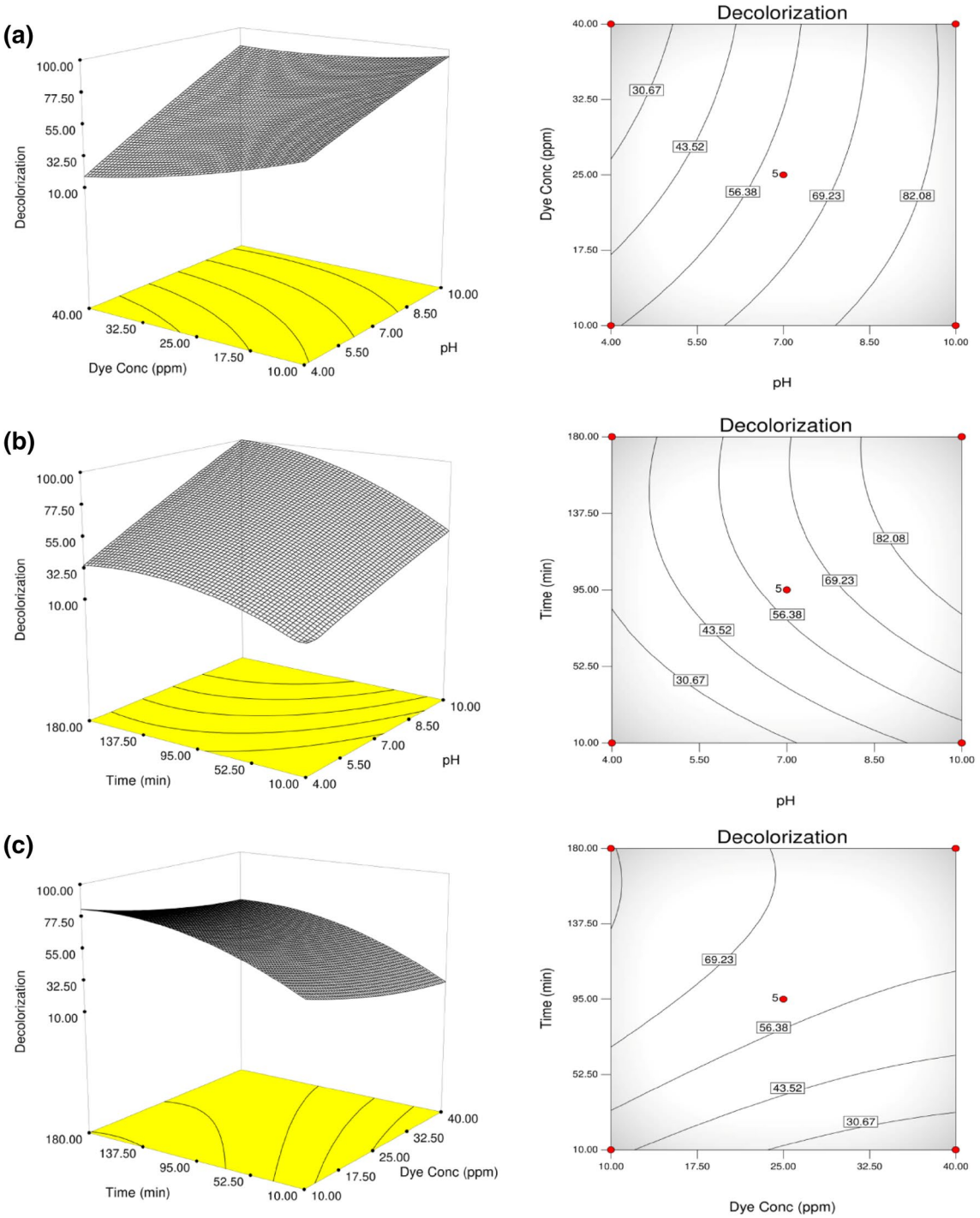

Fig. 5 3D response surfaces plots and 2D contour plots of the interaction effects between **a** pH and initial MB concentration (at constant $t = 95$ min), **b** pH and irradiation time (at constant initial MB conc.=25 ppm) and **c** irradiation time and initial MB concentration (at constant ~ 8 pH)

to 173 min. Under optimized conditions, the dye removal appears to follow the first order reaction, which is typically the case with several other organic compounds. To confirm the model suitability, a series of seven experiments were conducted and results were compared with predicted ones (Table-S4, Supporting Info). We obtained a comparable decolorization efficiency (%) ranges from 96.92 ± 0.41 to 98.63 ± 0.12 which confirms the legitimacy of the generated model for stimulating MB decolorization by biologically synthesized silver nanoparticles.

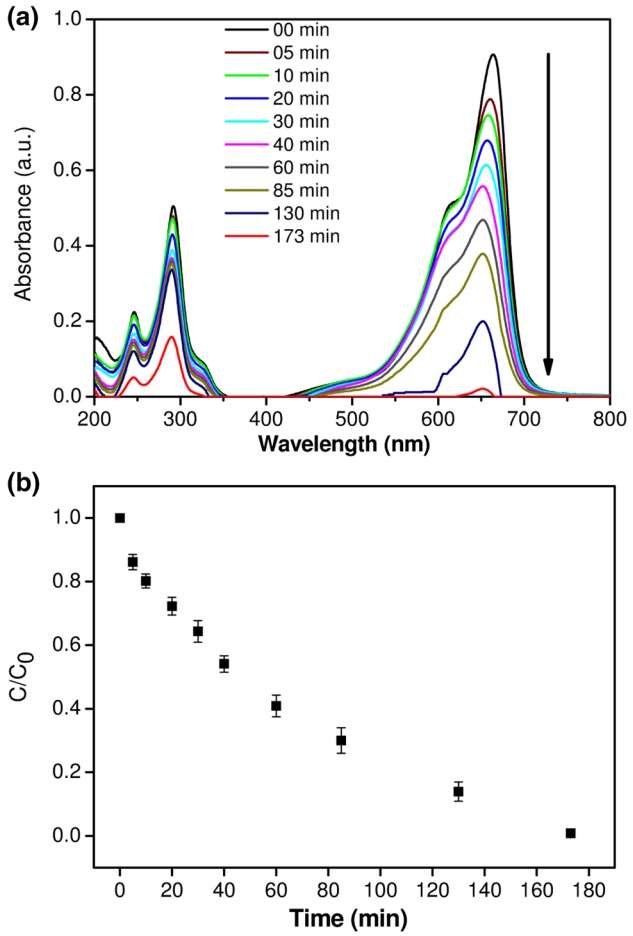

Fig. 6 **a** UV–Visible adsorption spectra demonstrating dye decolorization under optimized conditions. **b** A plot of C/C_0 vs reaction time for photocatalytic removal of methylene blue

Kinetic models are utilized as a tool while designing photocatalytic decolorization of dye at pilot or large scale. To understand the decolorization of dye and its mechanism, four types of kinetic models i.e., first order, pseudo-first order, second order, and pseudo second order were evaluated (Fig. 7). The individual results and their corresponding k values are also presented in Table 2. Among all four models, the first order kinetics was fitted well with the highest correlation coefficient (R^2) of 0.996. First order kinetics illustrates that the rate of reaction is proportional to the substrate depletion. Since the R^2 value of either second order or pseudo second order models (Table 2) were far from the unity, it shows that none of them were found suitable to dictate the decolorization rate. Surprisingly, in contrast to several earlier reports, a pseudo-first order kinetics was also not fitted well ($R^2 = 0.798$) which indicates that there might some other mechanism(s), which is playing key role in photocatalytic removal other than surface catalysis.

Another kinetic-diffusion based model, i.e., intraparticle diffusion was tested to check whether pore diffusion is the rate-limiting step of the adsorption process. This model assumes that a plot of MB removal varies linearly with the square root of irradiation time. As shown in Fig. 7e, the process of intraparticle diffusion ($R^2 = 0.980$) appeared to participate as a subsidiary mechanism for MB removal other than the first order kinetics, which was continued up to a duration of 130 min. From the curve, the rate of intraparticle diffusion was estimated as 3.791 mg L^{-1} $min^{-0.5}$ while the intercept on y-axis (c_i) was calculated as 1.495, which is proportional to the boundary layer thickness (Ayad and El-Nasr 2010). It was not surprising to see that the linear slope did not pass through the origin, which precludes the possibility of intraparticle diffusion to be the rate-limiting step in the removal kinetics of MB. Rather, the photocatalytic degradation and intraparticle diffusion were expected to work concurrently for the efficient removal of methylene blue where the segregated contributions of both mechanisms were difficult to explain.

Antibacterial activity

The antibacterial activity of as synthesized AgNPs were tested against Gram-positive *Bacillus subtilis* and Gram-negative *Pseudomonas aeruginosa* strains, which are known to cause nosocomial infections (Agnihotri and Dhiman 2017; Agnihotri et al. 2018). At a concentration 2.50 µg mL^{-1} and above, AgNPs showed a clear zone of inhibition (ZoI) ranging from 8 to 11 mm against both strains type (Fig. S2, Supporting info). A positive control containing only PW extract (devoid of AgNPs) did not show any ZoI. This indicates that the biocidal effect to prevent bacterial contamination was manifested specifically due to AgNPs alone. Since the antibacterial effectiveness of AgNPs was found to be comparable against both the strains (i.e., similar diameter of ZoI) in agar plate assay, liquid broth dilution assay were performed to evaluate strain-specific antibacterial activity. For instance, AgNPs with concentration 0.6, 1.25, 2.5, 5, 7.5, 10, and 20 µg mL^{-1} were introduced into a high bacterial population (10^5 CFU mL^{-1}, 100 mL) and incubated at 37 °C overnight. Regardless of strain type, the bacterial concentration decreased continuously while increasing AgNPs concentration. At 5.0 µg mL^{-1} concentration of AgNPs, the microbial growth of both strains was completely inhibited, indicating this value as their minimum inhibitory concentration (MIC). In later experiments, the minimum bactericidal concentration (MBC) values of AgNPs against *B. subtilis* and *P. aeruginosa* strains were determined as 7.5 and 5.0 µg mL^{-1}, respectively (Table 3), which demonstrated that AgNPs were more effective against Gram-negative strains.

Furthermore, the biocidal performance of biogenic AgNPs was compared under light and dark conditions. As shown in Table 3, without any exception, the amount of proteins released from the AgNP-treated cells was higher

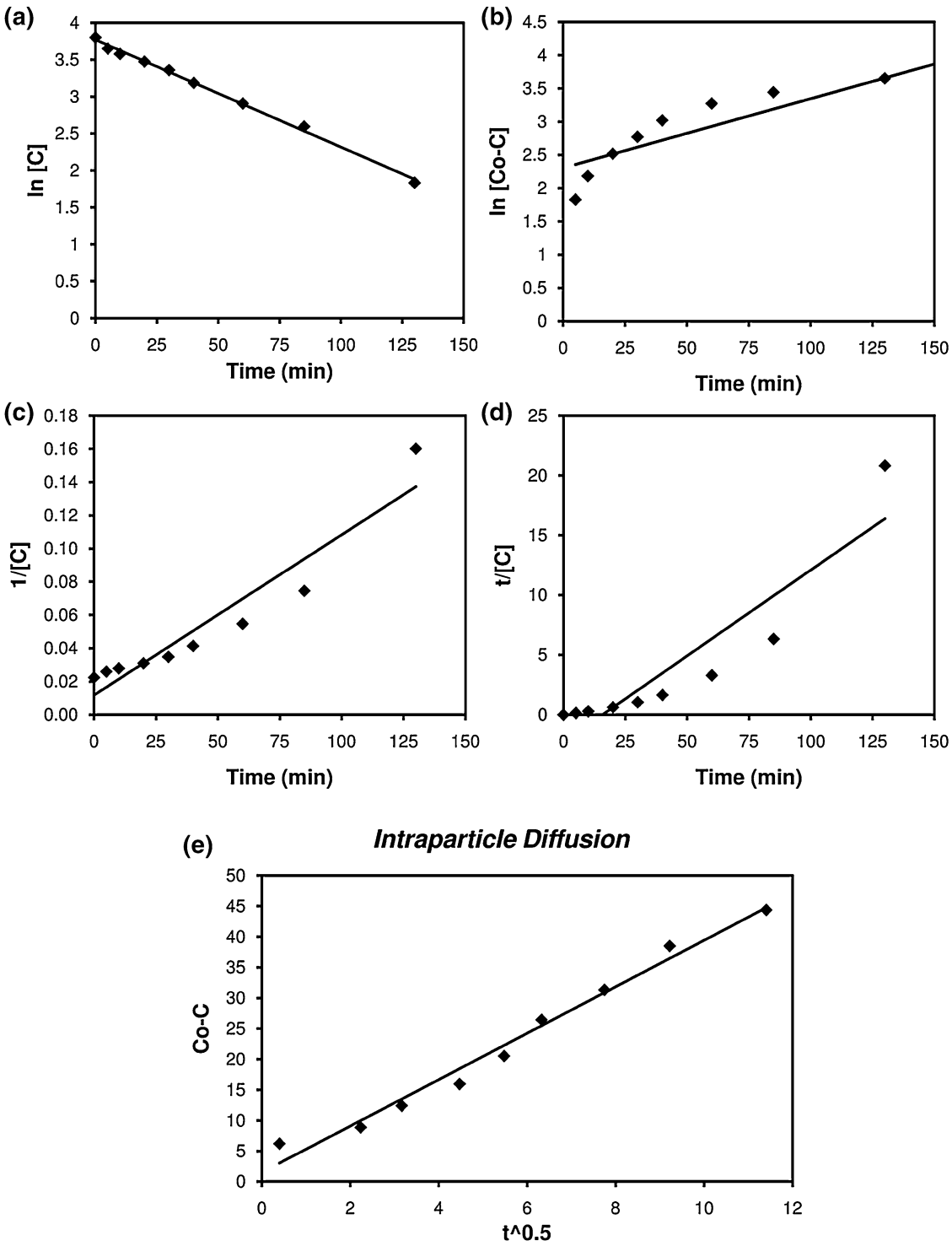

Fig. 7 Model fitting for the photocatalytic decolorization of MB following (a) first order (b) pseudo-first order (c) second order (d) pseudo-second order and (e) intraparticle diffusion model(s)

than the untreated (control) cells which can be ascribed to the role of AgNPs increasing membrane permeability. Irrespective of the light conditions, gram-negative *P. aeruginosa* were found be more sensitive towards AgNPs than the Gram-positive *B. subtilis* strains which resulted in more amount of proteins leakage. This can be well explained by the presence of additional peptidoglycan layers in the cell wall of Gram-positive bacteria which

Table 2 Kinetic parameters for decolorization of MB on AgNPs under sunlight illumination (32–35 °C), Initial MB conc. 40 ppm, and Initial AgNP conc. 1 mM at working pH ~ 10

Models	Equation	Rate constant, k	R^2 values
First order	$\ln C = \ln C_0 - kt$	14×10^{-3} min^{-1}	0.996
Pseudo-first order	$\ln[C_0 - C] = \ln C - kt$	10×10^{-3} min^{-1}	0.798
Second order	$\frac{1}{C} = \frac{1}{C_0} + kt$	0.5×10^{-3} mg^{-1} L min^{-1}	0.876
Pseudo-second order	$\frac{t}{C} = \frac{t}{C_0} - \frac{1}{kC_0^2}$	0.8×10^{-3} mg^{-1} L min^{-1}	0.845
Intraparticle diffusion	$\left[C_0 - C\right] = kt^{1/2} + c_i$	3.791 mg L^{-1} min$^{-0.5}$	0.980

C_0 initial concentration of dye, C final concentration dye, t time, k rate constant

Table 3 Strain-specific antibacterial potential of silver nanoparticles

Organisms	ZoI (mm)	MIC (μg ml^{-1})	MBC (μg ml^{-1})	Total proteins leakage from bacterial cells (μg ml^{-1})‡		
				Untreated cells (Control)	AgNP-treated cells (under Dark)	AgNPs treated cells (under Sunlight)
B. subtilis	8–11	5.0	7.5	305 ± 8	341 ± 7	359 ± 12
P. aeruginosa	8–11	5.0	5.0	361 ± 9	416 ± 16	483 ± 11

ZoI zone of inhibition, *MIC* minimum inhibitory conc., *MBC* minimum bactericidal conc.

analyses were done in tripliAll analyses were done in triplicates and the average value ± SE is represented demonstrating a significant difference at α = 0.05 levels (Duncan's multiple range test)

provide them an inherent defense mechanism to withstand harsh conditions.

For both strain types, the exposure of AgNP-treated cells under sunlight illumination resulted in more amount of proteins leakage from cells as compared to when exposed to the dark conditions. Results clearly demonstrate that the photocatalytic efficacy of AgNPs was increased by 16.1% and 5% in case with *B. subtilis* and *P. aeruginosa*, respectively, in the presence of visible light conditions. The analyses corroborates well with previous studies (Li et al. 2012; Rivas Aiello et al. 2016), where the production of reactive oxygen species (ROS) contributed towards the enhanced biocidal activity of AgNPs. Moreover, the generation of hydroxyl free radicals (OH·) during photochemical reactions can be postulated as the major ROS for antibacterial effects, which have been validated in earlier sections (dye decolorization studies). Nevertheless, the contribution of other mechanisms like AgNP internalization within the cells, formation of pits and hole in cell wall, and AgNP-proteins/AgNP-DNA interactions cannot be ignored completely (Sharma et al. 2009; Agnihotri et al. 2013, 2014; Mukherji et al. 2012). We hypothesize that these subsidiary pathways to AgNPs toxicity would be facilitated by an initial increase in membrane permeability under sunlight illumination, which resulted into a manifold increase in its effectiveness to kill these pathogens.

Conclusion

The biogenic synthesis of AgNPs from pineapple peel waste extract (*Ananas comosus*) has emerged as a convenient, cost-effective and eco-friendly substitute over chemical synthesis which produces size-controlled and monodispersed nanoparticles with ultra high stability. Our investigation on their photocatalytic performance indicated that AgNPs can degrade organic molecules including complex dyes under natural sunlight conditions. At alkaline pH, the higher degradation of MB dye was in good accord with restricted oxidative dissolution and stabilization of Ag_2O layers over AgNP surface, which controlled the release of Ag^+ while maintaining their colloidal stability. Through process optimization and modeling kinetics, we conceptualize the fact that it is possible to decolorize MB completely under practically relevant conditions where more than one mechanism would work synergistically to achieve the desired effect. Biogenic AgNPs were equally effective against *Pseudomonas aeruginosa* and *Bacillus subtilis* pathogenic strains demonstrating clear zone of inhibition, and comparable MIC and MIB values with that of the standard antibiotics. The antibacterial property of biogenic AgNPs is envisaged due to the generation of ROS which acted synergistically with increasing membrane permeability. We also anticipated that the production of free radicals could have also triggered the other mechanisms of AgNP's toxicity (internalization of NPs, formation of

pits/hole in cell wall, inhibiting mitochondrial machinery), which lead to a greater biocidal efficacy. This development will solve three major environmental issues: (1) utilization of pineapple waste for synthesizing a value-added product, i.e., AgNPs (2) minimization of waste disposal, and (3) harnessing natural resources to degrade organic compounds and improving personal hygiene.

Acknowledgements DS extends his grateful thanks to DST-SERB for the financial assistance as JRF. This work was supported as a Start Up Research Grant (Young Scientist) by the Department of Science and Technology (DST-SERB) New Delhi, India under the Project Grants Code: YSS/2015/001599, dated 23.03.2016 in Engineering Sciences.

Compliance with ethical standards

Conflict of interest The authors declare no conflict of interest.

References

Agnihotri S, Dhiman NK (2017) Development of nano-antimicrobial biomaterials for biomedical applications. In: Tripathi A, Melo JS (eds) Advances in biomaterials for biomedical applications. Springer, Singapore, pp 479–545. https://doi.org/10.1007/978-981-10-3328-5_12

Agnihotri S, Mukherji S, Mukherji S (2012) Antimicrobial chitosan–PVA hydrogel as a nanoreactor and immobilizing matrix for silver nanoparticles. Appl Nanosci 2(3):179–188

Agnihotri S, Mukherji S, Mukherji S (2013) Immobilized silver nanoparticles enhance contact killing and show highest efficacy: elucidation of the mechanism of bactericidal action of silver. Nanoscale 5(16):7328–7340. https://doi.org/10.1039/C3nr00024a

Agnihotri S, Mukherji S, Mukherji S (2014) Size-controlled silver nanoparticles synthesized over the range 5–100 nm using the same protocol and their antibacterial efficacy. RSC Adv 4(8):3974–3983

Agnihotri S, Bajaj G, Mukherji S, Mukherji S (2015) Arginine-assisted immobilization of silver nanoparticles on ZnO nanorods: an enhanced and reusable antibacterial substrate without human cell cytotoxicity. Nanoscale 7(16):7415–7429

Agnihotri S, Dhiman NK, Tripathi A (2018) Antimicrobial surface modification of polymeric biomaterials In: Tiwari A (ed) Handbook of antimicrobial coatings. Elsevier, New York, pp 435–486. https://doi.org/10.1016/B978-0-12-811982-2.00020-2

Akerdi AG, Bahrami SH, Arami M, Pajootan E (2016) Photocatalytic discoloration of Acid Red 14 aqueous solution using titania nanoparticles immobilized on graphene oxide fabricated plate. Chemosphere 159:293–299

Akhtar MS, Panwar J, Yun Y-S (2013) Biogenic synthesis of metallic nanoparticles by plant extracts. ACS Sustain Chem Eng 1(6):591–602. https://doi.org/10.1021/sc300118u

Awazu K, Fujimaki M, Rockstuhl C, Tominaga J, Murakami H, Ohki Y, Yoshida N, Watanabe T (2008) A plasmonic photocatalyst consisting of silver nanoparticles embedded in titanium dioxide. J Am Chem Soc 130(5):1676–1680. https://doi.org/10.1021/ja076503n

Ayad MM, El-Nasr AA (2010) Adsorption of cationic dye (Methylene blue) from water using polyaniline nanotubes base. J Phys Chem C 114(34):14377–14383. https://doi.org/10.1021/jp103780w

Bharti S, Agnihotri S, Mukherji S, Mukherji S (2015) Effectiveness of immobilized silver nanoparticles in inactivation of pathogenic bacteria. J Environ Res Dev 9(3A):849–856

Forgacs E, Cserhati T, Oros G (2004) Removal of synthetic dyes from wastewaters: a review. Environ Int 30(7):953–971

Ginimuge PR, Jyothi SD (2010) Methylene blue: revisited. J Anaesthesiol Clin Pharmacol 26(4):517–520

Hai FI, Yamamoto K, Fukushi K (2007) Hybrid treatment systems for dye wastewater. Crit Rev Environ Sci Technol 37(4):315–377

Hao OJ, Kim H, Chiang P-C (2000) Decolorization of wastewater. Crit Rev Environ Sci Technol 30(4):449–505. https://doi.org/10.1080/10643380091184237

He S, Yao J, Jiang P, Shi D, Zhang H, Xie S, Pang S, Gao H (2001) Formation of silver nanoparticles and self-assembled two-dimensional ordered superlattice. Langmuir 17(5):1571–1575

Hogan NJ, Urban AS, Ayala-Orozco C, Pimpinelli A, Nordlander P, Halas NJ (2014) Nanoparticles heat through light localization. Nano Lett 14(8):4640–4645

Hossain MA, Rahman SM (2011) Total phenolics, flavonoids and antioxidant activity of tropical fruit pineapple. Food Res Int 44(3):672–676

Kasuya A, Sivamohan R, Barnakov YA, Dmitruk IM, Nirasawa T, Romanyuk VR, Kumar V, Mamykin SV, Tohji K, Jeyadevan B (2004) Ultra-stable nanoparticles of CdSe revealed from mass spectrometry. Nat Mater 3(2):99

Khan S, Malik A (2018) Toxicity evaluation of textile effluents and role of native soil bacterium in biodegradation of a textile dye. Environ Sci Pollut Res 25(5):4446–4458. https://doi.org/10.1007/s11356-017-0783-7

Kora AJ, Beedu SR, Jayaraman A (2012) Size-controlled green synthesis of silver nanoparticles mediated by gum ghatti (*Anogeissus latifolia*) and its biological activity. Org Med Chem Lett 2:17–17. https://doi.org/10.1186/2191-2858-2-17

Koyani RD, Sanghvi GV, Sharma RK, Rajput KS (2013) Contribution of lignin degrading enzymes in decolourisation and degradation of reactive textile dyes. Int Biodeterior Biodegrad 77:1–9

Lee KJ, Jun BH, Choi J, Lee YI, Joung J, Oh YS (2007) Environmentally friendly synthesis of organic-soluble silver nanoparticles for printed electronics. Nanotechnology 18(33):335601

Leng K, Mai W, Zhang X, Liu R, Lin X, Huang J, Lou H, Xie Y, Fu R, Wu D (2018) Construction of functional nanonetwork-structured carbon nitride with Au nanoparticle yolks for highly efficient photocatalytic applications. Chem Commun 54:7159–7162. https://doi.org/10.1039/C8CC03095B

Li Y, Zhang W, Niu J, Chen Y (2012) Mechanism of photogenerated reactive oxygen species and correlation with the antibacterial properties of engineered metal-oxide nanoparticles. ACS Nano 6(6):5164–5173

Li X, Jin X, Zhao N, Angelidaki I, Zhang Y (2017) Novel bio-electro-Fenton technology for azo dye wastewater treatment using microbial reverse-electrodialysis electrolysis cell. Bioresour Technol 228:322–329. https://doi.org/10.1016/j.biortech.2016.12.114

Lin X, Liang Y, Lu Z, Lou H, Zhang X, Liu S, Zheng B, Liu R, Fu R, Wu D (2017) Mechanochemistry: a green, activation-free and top-down strategy to high-surface-area carbon materials. ACS Sustain Chem Eng 5(10):8535–8540

Lokesh K, Sivakiran R (2014) Biological methods of dye removal from textile effluents—a review. J Biochem Technol 3(5):177–180

Mittal AK, Chisti Y, Banerjee UC (2013) Synthesis of metallic nanoparticles using plant extracts. Biotechnol Adv 31(2):346–356. https://doi.org/10.1016/j.biotechadv.2013.01.003

Mukherjee P, Ahmad A, Mandal D, Senapati S, Sainkar SR, Khan MI, Parishcha R, Ajaykumar P, Alam M, Kumar R (2001) Fungus-mediated synthesis of silver nanoparticles and their immobilization in the mycelial matrix: a novel biological approach to nanoparticle synthesis. Nano Lett 1(10):515–519

Mukherjee P, Roy M, Mandal B, Dey G, Mukherjee P, Ghatak J, Tyagi A, Kale S (2008) Green synthesis of highly stabilized

nanocrystalline silver particles by a non-pathogenic and agriculturally important fungus *T. asperellum*. Nanotechnology 19(7):075103

Mukherji S, Ruparelia J, Agnihotri S (2012) Antimicrobial activity of silver and copper nanoparticles: variation in sensitivity across various strains of bacteria and fungi. In: Cioffi N, Rai M (eds) Nano-antimicrobials: progress and prospects. Springer-Verlag, Berlin Heidelberg, pp 225–251

Nadagouda MN, Iyanna N, Lalley J, Han C, Dionysiou DD, Varma RS (2014) Synthesis of silver and gold nanoparticles using antioxidants from blackberry, blueberry, pomegranate, and turmeric extracts. ACS Sustain Chem Eng 2(7):1717–1723. https://doi.org/10.1021/sc500237k

Peng S, McMahon JM, Schatz GC, Gray SK, Sun Y (2010) Reversing the size-dependence of surface plasmon resonances. Proc Natl Acad Sci USA 107(33):14530–14534. https://doi.org/10.1073/pnas.1007524107

Peretyazhko TS, Zhang Q, Colvin VL (2014) Size-controlled dissolution of silver nanoparticles at neutral and acidic pH conditions: kinetics and size changes. Environ Sci Technol 48(20):11954–11961. https://doi.org/10.1021/es5023202

Raveendran P, Fu J, Wallen SL (2003) Completely "green" synthesis and stabilization of metal nanoparticles. J Am Chem Soc 125(46):13940–13941

Rivas Aiello MB, Romero JJ, Bertolotti SG, Gonzalez MnC, Mártire DO (2016) Effect of silver nanoparticles on the photophysics of riboflavin: consequences on the ROS generation. J Phys Chem C 120(38):21967–21975. https://doi.org/10.1021/acs.jpcc.6b06385

Robinson T, McMullan G, Marchant R, Nigam P (2001) Remediation of dyes in textile effluent: a critical review on current treatment technologies with a proposed alternative. Bioresour Technol 77(3):247–255

Sahoo C, Gupta AK (2012) Optimization of photocatalytic degradation of methyl blue using silver ion doped titanium dioxide by combination of experimental design and response surface approach. J Hazard Mater 215–216:302–310. https://doi.org/10.1016/j.jhazmat.2012.02.072

Saraswaty V, Risdian C, Primadona I, Andriyani R, Andayani DGS, Mozef T (2017) Pineapple peel wastes as a potential source of antioxidant compounds. IOP Conf Ser Earth Environ Sci 60(1):012013

Saratale RG, Karuppusamy I, Saratale GD, Pugazhendhi A, Kumar G, Park Y, Ghodake GS, Bhargava RN, Banu JR, Shin HS (2018) A comprehensive review on green nanomaterials using biological systems: recent perception and their future applications. Colloids Surf B Biointerfaces 170(1):20–35. https://doi.org/10.1016/j.colsurfb.2018.05.045

Shanker U, Rani M, Jassal V (2017) Degradation of hazardous organic dyes in water by nanomaterials. Environ Chem Lett 15(4):623–642. https://doi.org/10.1007/s10311-017-0650-2

Sharma VK, Yngard RA, Lin Y (2009) Silver nanoparticles: green synthesis and their antimicrobial activities. Adv Colloid Interf 145(1–2):83–96

Sharma VK, Filip J, Zboril R, Varma RS (2015) Natural inorganic nanoparticles—formation, fate, and toxicity in the environment. Chem Soc Rev 44(23):8410–8423. https://doi.org/10.1039/C5CS00236B

Tayade RJ, Natarajan TS, Bajaj HC (2009) Photocatalytic degradation of methylene blue dye using ultraviolet light emitting diodes. Ind Eng Chem Res 48(23):10262–10267. https://doi.org/10.1021/ie9012437

Thanh NTK, Maclean N, Mahiddine S (2014) Mechanisms of nucleation and growth of nanoparticles in solution. Chem Rev 114(15):7610–7630. https://doi.org/10.1021/cr400544s

Tokitomo Y, Steinhaus M, Buttner A, Schieberle P (2005) Odor-active constituents in fresh pineapple (*Ananas comosus* [L.] Merr.) by quantitative and sensory evaluation. Biosci Biotechnol Biochem 69(7):1323–1330

Vikrant K, Giri BS, Raza N, Roy K, Kim KH, Rai BN, Singh RS (2018) Recent advancements in bioremediation of dye: current status and challenges. Bioresour Technol 253:355–367. https://doi.org/10.1016/j.biortech.2018.01.029

Wei C-B, Liu S-H, Liu Y-G, Lv L-L, Yang W-X, Sun G-M (2011) Characteristic aroma compounds from different pineapple parts. Molecules 16(6):5104–5112

Zhang W, Wu CW (2014) Dyeing of multiple types of fabrics with a single reactive azo disperse dye. Chem Pap 68(3):330–335. https://doi.org/10.2478/s11696-013-0444-3